Strong Hα emission in the young planetary mass companion 2MASS J0249−0557 c

P. Chinchilla[1,2], V. J. S. Béjar[1,2], N. Lodieu[1,2], M. R. Zapatero Osorio[3], and B. Gauza[4,5]

[1] Instituto de Astrofísica de Canarias (IAC), Calle Vía Láctea s/n, 38200 La Laguna, Tenerife, Spain.
   e-mail: pchinchilla.astro@gmail.com
[2] Departamento de Astrofísica, Universidad de La Laguna (ULL), 38205 La Laguna, Tenerife, Spain.
[3] Centro de Astrobiología (CSIC-INTA), Ctra. de Ajalvir km 4, 28850 Torrejón de Ardoz, Madrid, Spain.
[4] Centre for Astrophysics Research, University of Hertfordshire, College Lane, Hatfield AL10 9AB, UK.
[5] Janusz Gil Institute of Astronomy, University of Zielona Góra, Lubuska 2, 65-265 Zielona Góra, Poland.

ABSTRACT

Aims. Our objective is the optical and near-infrared spectroscopic characterisation of 2MASS J0249−0557 c, a recently discovered young planetary mass companion to the β Pictoris (∼25 Myr) member 2MASS J0249−0557.
Methods. Using the Visible and Infrared Survey Telescope for Astronomy (VISTA) Hemisphere Survey (VHS) and the Two Micron All Sky Survey (2MASS) data, we independently identified the companion 2MASS J0249−0557 c. We also obtained low-resolution optical spectroscopy of this object using the Optical System for Imaging and low-intermediate-Resolution Integrated Spectroscopy (OSIRIS) spectrograph at the Gran Telescopio Canarias (GTC), and near-infrared spectroscopy using the Son of Isaac (SofI) spectrograph on the New Technology Telescope (NTT).
Results. We classified 2MASS J0249−0557 c with a spectral type of L2.5±0.5 in the optical and L3±1 in the near-infrared. We identified several spectroscopic indicators of youth both in the optical and in the near-infrared that are compatible with the age of the β Pictoris moving group: strong absorption due to oxides, weak alkaline atomic lines, and a triangular shape of the *H*-band pseudo-continuum. We also detect a strong Hα emission, with a pseudo-equivalent width (pEW) of -90^{+20}_{-40}Å, which seems persistent at timescales from several days to a few years. This indicates strong chromospheric activity or disk accretion. Although many M-type brown dwarfs have strong Hα emission, this target is one of the very few L-type planetary mass objects in which this strong Hα emission has been detected. Lithium absorption at 6708 Å is observed with pEW $\lesssim$ 5 Å. We also computed the binding energy of 2MASS J0249−0557 c and obtained an (absolute) upper limit of $U = (-8.8 \pm 4.4)10^{32}$ J.
Conclusions. Similarly to other young brown dwarfs and isolated planetary mass objects, strong Hα emission due to accretion or chromospheric activity is also present in young planetary mass companions at ages of some dozen million years. We also found that 2MASS J0249−0557 c is one of the wide substellar companions with the lowest binding energy known to date.

Key words. brown dwarfs – planetary systems – binaries:visual – open clusters and associations: individual: β Pictoris – Stars: pre-main sequence

1. Introduction

One of the main challenges in astronomy today is understanding the formation and evolution of planetary systems. The characterisation of planets of different ages is key to providing a more accurate picture of the different stages of their formation. However, this characterisation is very difficult because planets are frequently too close to their parent stars and are too faint compared to them to be directly imaged. One possible solution for this issue is finding wide (>50–100 AU) planetary mass companions, which can serve as analogues to the close-orbit giant planets. Because these objects have a wide separation from their primary star, they can be fully characterised using spectroscopy (e.g. Aller et al. 2013; Bowler et al. 2014; Deacon et al. 2014; Gauza et al. 2015; Dupuy et al. 2018; Chinchilla et al. 2020).

β Pictoris is a young moving group (YMG) named after its brightest and most famous member, the A-type star β Pictoris. The group was first discovered by Zuckerman et al. (2001), who identified 17 young stellar systems moving through space together with the main representative of the group. With an age of ∼20–25 Myr (Barrado y Navascués et al. 1999; Mentuch et al. 2008; Binks & Jeffries 2014; Malo et al. 2014; Mamajek & Bell

2014; Bell et al. 2015; Shkolnik et al. 2017) and a mean heliocentric distance of ∼40 pc (Miret-Roig et al. 2018), its youth and proximity make the β Pictoris YMG one of the best laboratories for the search and characterisation of young substellar companions.

One of the most recently discovered wide planetary mass companions is 2MASS J02495436−0558015 (hereafter 2MASS J0249−0557 c; Dupuy et al. 2018). This is a $11.6^{+1.3}_{-1.0}$ M_{Jup} object orbiting at a separation of ∼1950 AU from the M6 member of β Pictoris YMG 2MASS J02495639−0557352. The primary itself has been resolved by the Keck Laser Guide Star (LGS) adaptive optics into a close (2.17±0.22 AU, 0.04″) brown dwarf pair (hereafter 2MASS J0249−0557 AB), with estimated masses of $48^{+13}_{-12.0}$ M_{Jup} and $44^{+14}_{-11.0}$ M_{Jup}, respectively (Dupuy et al. 2018).

We present the independent discovery and new optical and near-infrared characterisation of 2MASS J0249−0557 c. Section 2 describes the main characteristics of the system. In Section 3 we present the independent identification of this object. Section 4 describes the optical and near-infrared spectroscopic observations obtained for the planetary mass companion, and section 5
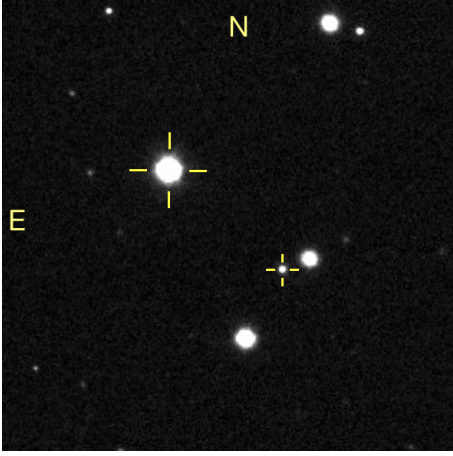
Fig. 1. *J*-band VHS finding chart for the 2MASS J0249−0557 system. The system components are marked with crosses. The field of view is 2′× 2′and the orientation is north up and east to the left. The angular separation between the components is 40.0″.

Fig. 2. Proper motion diagram for 2MASS J0249−0557 AB (light pink) and 2MASS J0249−0557 c (red) from the VHS–2MASS cross correlation. Other cross-correlated objects in the same field of view are marked in grey.

Fig. 3. M_J vs. $J-Ks$ colour-magnitude diagram for 2MASS J0249−0557 AB (light pink) and 2MASS J0249−0557 c (red). Other known β Pic members are plotted as grey dots. The photometric sequence of field dwarfs derived by Pecaut & Mamajek (2013, squares), Dupuy & Liu (2012, triangles), and Lodieu et al. (2014, diamonds) is also shown in purple.

presents the main results. Finally, Section 6 provides the summary and final remarks.
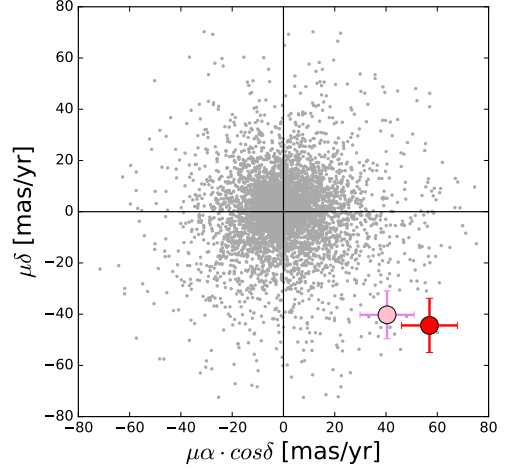
2. 2MASS J0249−0557 system

The primary, 2MASS J0249−0557, was included in Shkolnik et al. (2017) as a new confirmed member of β Pic moving group. They determined a spectral type of M6 and found very low gravity signs in its near-infrared spectrum. They measured a radial velocity of 14.42 ± 0.44 km s^{-1}, a lithium pseudo-equivalent width (pEW) of 0.59±0.05 Å and a strong Hα emission line with a pEW of −11.6±0.1 Å.

Dupuy et al. (2018) recently published the discovery of 2MASS J0249−0557 c as a wide (39.959±0.005″, 1950±200 AU) companion to 2MASS J0249−0557, one of the targets from the Hawaii Infrared Parallax Program. They also found that the primary is a tight brown dwarf binary, revealing that 2MASS J0249−0557ABc is a bound triple system. Using the Keck/NIRC2 instrument and the laser guide star adaptive optic system (LGS AO), they resolved the primary into two similar magnitude objects located at an angular separation of 44.4±2 mas (equivalent to 2.17±0.22 AU). They determined a near-infrared spectral type of L2 VL-G for the wide companion and masses of 48^{+13}_{-12} and 44^{+14}_{-11} M$_{Jup}$ for the tight binary and $11.6^{+1.3}_{-1.0}$ M$_{Jup}$ for the wide companion. They measured the parallax and proper motions, and confirmed the membership of this system in the β Pic moving group. They showed that the companion 2MASS J0249−0557 c is physically bound, which means that this is one of the few triple substellar systems known to date.

3. Independent identification of 2MASS J0249−0557 c

As part of our efforts to characterise the frequency of wide substellar companions around young nearby stars, we performed a search for common proper motion companions to known members and candidate members of the β Pictoris YMG, among other young stellar kinematic groups, using data from the Visible and Infrared Survey Telescope for Astronomy (VISTA) Hemisphere Survey (VHS, McMahon et al. 2013) catalogue in combination
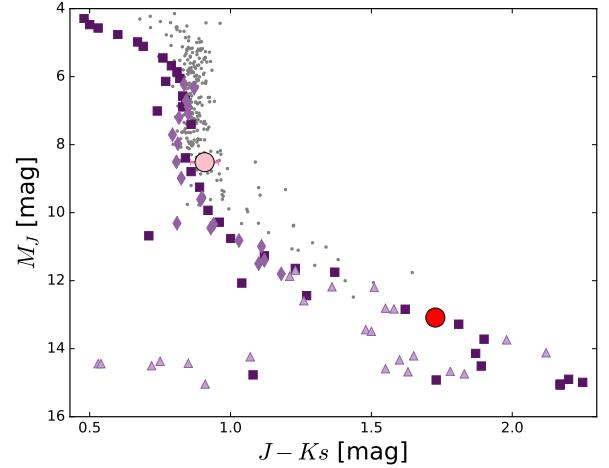
with the Two Micron All-Sky Survey (2MASS, Skrutskie et al. 2006) catalogue.

For this purpose, we first compiled a list of 348 known members and candidate members of β Pictoris, which we obtained from Schlieder et al. (2010, 2012), Malo et al. (2013), Bell et al. (2015), Best et al. (2015), Gagné et al. (2015a), Gagné et al. (2015b), Elliott et al. (2016), Messina et al. (2017), Schneider et al. (2017), Shkolnik et al. (2017) and Gagné & Faherty (2018). One of the members in this list is 2MASS J0249−0557.

Secondly, we queried the VHS database to download all the available data in a circular area corresponding to 50 000 AU around each β Pic candidate member in the compilation. The angular area corresponding to this radius was calculated in most of the cases using the available parallaxes from *Gaia* DR2. For the objects without parallaxes, we downloaded all the data in

a 83.4′ radius, which corresponds to a physical separation of 50 000 AU for an object placed at 10 pc distance, considering this as a lower limit for the heliocentric distance of β Pic members.

Then, we cross-matched the VHS data with the 2MASS catalogue to identify nearby objects whose proper motions matched those of the primaries within an error of 40 mas yr^{-1} in total. This value is at least twice the typical dispersion in the measured proper motions of non-moving background objects, which is 10–20 mas yr^{-1}, depending on the time baseline between the VHS and 2MASS observations (9–19 years). To the targets with compatible proper motions, we later applied photometric selection criteria using VHS and 2MASS (Skrutskie et al. 2006) photometry and also DENIS and/or AllWISE data (Epchtein et al. 1997; Wright et al. 2010) when available. We selected as good candidate companions those objects whose magnitudes and colours followed a well-defined photometric sequence with their primaries in different colour-magnitude diagrams, and which therefore can be placed at the same heliocentric distance. We also used *Gaia* DR2 (Gaia Collaboration et al. 2016, 2018) astrometry for the brightest candidates to discard chance alignments.

As a result of this search, we found 2MASS J0249−0557 c, placed at a distance of 39.947±0.014 arcsec from 2MASS J0249−0557, with a position angle of 228.°644 ± 0.°020. These measured separation and position angles are compatible with those published in Dupuy et al. (2018). This is the faintest candidate companion identified in our search. However, because we are limited to the completeness of 2MASS ($J\sim16$) in this search, other candidate companions with similar masses and spectral types may have remained undetected. Figure 1 shows the finding chart for the 2MASS J0249−0557 system. The proper motion of the candidate companion agreed well with the motion of the primary, and its magnitude and colours were consistent with an L-type object located at the same heliocentric distance as the primary brown dwarf pair. Figures 2 and 3 show the proper motion diagram and J–J-Ks colour magnitude diagram for the system.

2MASS J0249−0557 was imaged by VHS, 2MASS, Pan-STARRS (Chambers et al. 2016), the Sloan Digital Sky Survey (SDSS; York et al. 2000), WISE, and Gaia. The available photometric data for the system are presented in Table 1.

4. Follow-up observations and data reduction

4.1. GTC/OSIRIS optical spectroscopy

2MASS J0249−0557 c was observed on 27 January 2019 with the Optical System for Imaging and low-intermediate-Resolution Integrated Spectroscopy (OSIRIS; Cepa et al. 2000) spectrograph at the 10.4 m Gran Telescopio Canarias (GTC) in La Palma, Canary Islands. The observations were performed in long-slit spectroscopy mode, using the R500R grism (wavelength coverage 0.48–1.00 μm) and the 0.8″ wide slit placed in parallactic angle, providing a resolution of ∼440 at 7200 Å. Four exposures of 1600s were obtained using an ABBA nodding pattern with a 14″ offset along the slit. The object acquisition was performed using the Sloan z filter. The seeing value was 0.7″. The spectrophotometric standard G191-B2B (DA white dwarf, V=11.7) was also observed with the same instrumental configuration to correct for the instrumental response. The observation log is shown in Table 2.

The data reduction was performed using standard routines within the Image Reduction and Analysis Facility (IRAF) environment (Tody 1986, 1993). The images were corrected for

Table 1. General data of 2MASS J0249−0557 AB and c.

Astrometry	AB	c
R.A. (J2000)	02 : 49 : 56.39	02 : 49 : 54.36
DEC (J2000)	−05 : 57 : 35.2	−05 : 58 : 01.5
Parallax (mas) [a]	20.5 ± 2.1	20.1 ± 3.5
Distance (pc) [a]	48.9$^{+4.4}_{-5.4}$	
Separation (arcsec) [a]	0.0444 ± 0.0002″	39.959 ± 0.005″
Separation (AU) [a]	2.17 ± 0.22	1950 ± 200
P.M. (mas yr^{-1}) [a]	(42.9, −30.2)	(46.0, −32.0)
	±(2.0, 1.8)	±(2.3, 2.1)
Spectroscopy		
Spectral type	M6 [b]	L2.5 ± 0.5 OPT, L3 ± 1 NIR [c]
Li pEW (Å)	0.59 ± 0.05 [b]	$\lesssim$ 5
Hα pEW (Å)	−11.61 ± 0.1 [b]	-90^{+20}_{-40} [c]
Photometry		
Gaia g	15.6894 ± 0.0012	–
SDSS u	21.47 ± 0.14	–
SDSS g	18.721 ± 0.008	–
SDSS r	17.197 ± 0.006	–
SDSS i	14.977 ± 0.005	20.76 ± 0.13
SDSS z	13.754 ± 0.005	19.28 ± 0.15
Pan-STARRS g	18.419 ± 0.008	–
Pan-STARRS r	17.145 ± 0.005	–
Pan-STARRS i	14.992 ± 0.004	21.36 ± 0.06
Pan-STARRS z	13.984 ± 0.004	19.92 ± 0.03
Pan-STARRS y	13.409 ± 0.004	18.93 ± 0.03
VHS J	11.9667 ± 0.0007	16.531 ± 0.008
VHS Ks	11.2535 ± 0.0009	14.804 ± 0.009
2MASS J	11.96 ± 0.03	16.55 ± 0.11
2MASS H	11.36 ± 0.03	15.48 ± 0.13
2MASS K	11.06 ± 0.02	14.88 ± 0.12
WISE w1	10.84 ± 0.02	14.13 ± 0.03
WISE w2	10.60 ± 0.02	13.59 ± 0.04
WISE w3	10.39 ± 0.06	–

Notes. [a] Data from Dupuy et al. (2018). [b] Data from Shkolnik et al. (2017). [c] Data from this work.

bias and were flat-fielded. Then, the 2D images of the four individual exposures of the target were corrected for bad pixels and cosmic rays using IMEDIT. The four target spectra and the spectrophotometric standard spectrum were extracted using the APALL routine. The spectra were wavelength calibrated at each nodding position using HgAr, Ne, and Xe arc images. The spectrum of the standard was corrected for second-order contamination of the light at wavelengths 4800–4900 Å using a spectrum taken with the z-band filter, following the procedure explained in Zapatero Osorio et al. (2014). We obtained the sensitivity function from the standard star spectrum. Then, the spectra of the target were corrected for instrumental response using this sensitivity function. Finally, for an optimal combination of the four spectra, the data were aligned in wavelength with respect to the first exposure by cross-correlating the observations (the regions with strong telluric absorption were excluded from the cross correlation). The final combined spectrum is shown in Figures 4 and 5.

4.2. NTT/SofI infrared spectroscopy

We obtained near-infrared low-resolution spectroscopy of 2MASS J0249−0557 c on 21 June 2018 and 4 November 2018

Table 2. Observation log for 2MASS J0249−0557 c

Obs. Date	Telesc/Instrum	Mode	Grating/ Filter	Wavelength Range [μm]	Slit ["]	Pl. Scale ["/pix]	Disp. [Å/pix]	Res. Power	Exp. Time [s]	Airmass	Seeing ["]
11 Sep 2016	VISTA/VIRCAM	Img	J, Ks	–	–	0.34	–	–	8×15, 8×7.5	1.1	0.9
21 Jun 2018	NTT/SofI	Spec	GR	1.53–2.52	1	0.29	10.22	600	4×300	1.4–1.5	0.9
21 Jun 2018	NTT/SofI	Spec	GB	0.95–1.64	1	0.29	6.96	600	4×600	1.6–1.8	0.9
4 Nov 2018	NTT/SofI	Spec	GR	1.53–2.52	1	0.29	10.22	600	4×300	1.2–1.3	0.6
4 Nov 2018	NTT/SofI	Spec	GB	0.95–1.64	1	0.29	6.96	600	4×600	1.1–1.2	0.6
27 Jan 2019	GTC/OSIRIS	Spec	R500R	0.48–1.00	0.8	0.25	4.88	440	4×1600	1.2–1.4	0.7

using the Son of Isaac (SofI) spectrograph (Moorwood et al. 1998) mounted on the 3.6 m New Technology Telescope (NTT) at the La Silla Observatory, Chile, to determine the spectral type of the candidate companion and search for features of youth. We used long-slit spectroscopy mode with the 1.0″ wide slit, and the low-resolution blue and red grisms (wavelength ranges 0.95–1.64 μm and 1.53–2.52 μm, respectively, resolving power 600, and nominal dispersion 6.96 and 10.22 Å pix^{-1}, respectively). The exposures were taken using an ABBA nodding pattern along the slit, with 600s and 300s individual exposure times in each position for blue and red grisms, respectively. We also observed the B7 telluric standards HIP14143 and HIP17457 after the exposures and at similar airmasses to correct for telluric absorption. To perform the flat-field correction and wavelength calibration, we also acquired continuum-lamp images and Xe arc-lamp images. A log of these observations is included in Table 2.

The data reduction was performed using the SofI pipeline by ESO within the Gasgano environment (Gebbinck & Sforna 2007) and standard IRAF routines for both the target and telluric standards. The raw spectroscopic images were flat-field and dark corrected, aligned, and combined using Gasgano. We then used the IRAF APALL routine to extract the spectra from these 2D combined images, and wavelength calibrated them using the Xe arcs. We manually removed the intrinsic lines of the spectrum of the telluric star. Finally, to correct for the instrumental response, the target spectra were divided by the telluric spectra and multiplied by a black body of 14 500 K, which is the corresponding temperature for the telluric star spectral type (Pecaut & Mamajek 2013). For a better result in the signal-to-noise ratio, we combined the resulting spectra from the two observations. The final spectrum is shown in Figures 6 and 7.

5. Results and discussion

5.1. Optical characterisation and spectral classification

We have compared the optical spectrum of 2MASS J0249−0557 c with several young and old L-dwarf templates to determine the optical spectral type and analyse its spectral features. Figure 4 shows the comparison between the GTC/OSIRIS optical spectrum of 2MASS J0249−0557 c and some old field L-type standards from Kirkpatrick et al. (1999) and Kirkpatrick et al. (2000), observed with the Low Resolution Imaging Spectrometer (LRIS) and the 400/8500 grism (R∼1100) on the Keck-I Telescope. LRIS spectra were convolved with a Gaussian to match the GTC/OSIRIS spectral resolution.

From this comparison, we find that the general spectral energy distribution of 2MASS J0249−0557 c in the optical fits that of the early and intermediate old-field L dwarfs. When we focus on the pseudo-continuum, the overall shape of the spectrum, particularly above 8000 Å, coincides with that of the intermedi-

ate old field dwarf of L5 spectral type. However, the depth of the VO, TiO, FeH, and CrH absorption bands in the optical spectrum of the target are better reproduced by early old field L dwarfs. These differences in the spectral features can be explained by the effect of the low gravity of the young object, which is still contracting. These discrepancies are frequent when young objects are compared with old counterparts, and can be misinterpreted as a difference in spectral type. For example, the shapes of the VO bands at 7300–7600 Å and 7800–8000 Å are closer in depth to the L1–L2 spectral templates. TiO at 8400–8600 Å is weakened and closer to later spectral types. This can also be seen at the 7000–7400 Å TiO band. Alkali lines are also weakened, as can be seen in the NaI doublet at 8183–8195 Å or in the CsI line at 8521 Å.
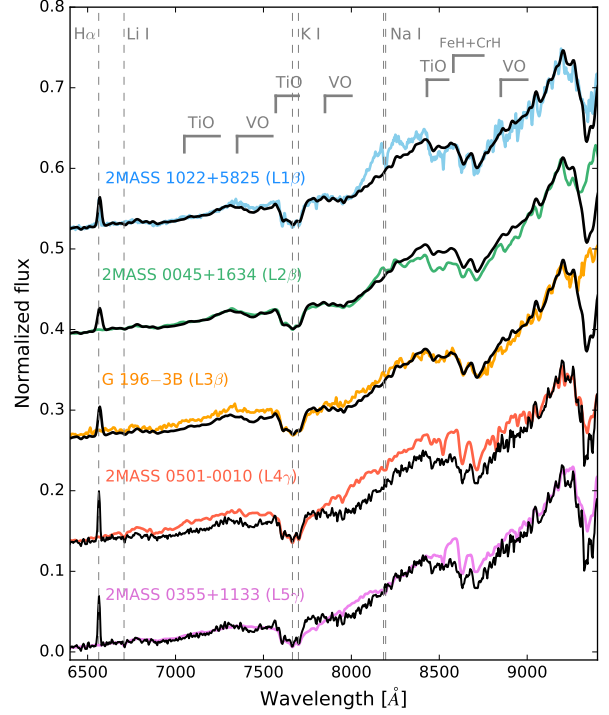
We also observed a tentative detection of the absorption line of Li I at 6708 Å, with a pEW of ≲ 5 Å. Nevertheless, the feature is barely distinguishable from the spectral noise at a 2σ level. The obtained value is compatible with a total preservation of lithium, as expected for a β Pictoris L2–3 member (Kirkpatrick et al. 2000).

For a more accurate spectral type classification, we also compared the optical spectrum of 2MASS J0249−0557 c to the spectra of some known young objects with spectral types L1–L5. Figure 5 shows these comparisons. This figure shows the strong resemblance of the spectrum of 2MASS J0249−0557 c to the optical spectra of 2MASS J00452143+1634446 (2MASS 0045+1634), which is classified as an L2, and G 196–3B (Rebolo et al. 1998), which is classified as an L3. 2MASS 0045+1634 is a young substellar object, with an estimated age of 10–100 Myr (Zapatero Osorio et al. 2014). It has been claimed as a likely member of the Argus moving group (40–50 Myr; Torres et al. 2008; Zuckerman 2019) by Gagné et al. (2014). G 196–3B is a young object, with an estimated age of 20–300 Myr, and it is also likely younger than 100 Myr (Zapatero Osorio et al. 2010, 2014). Gagné et al. (2014) indicated a moderate probability that G196–3B belongs to the AB Doradus moving group (∼125 Myr; Zuckerman et al. 2004; Luhman et al. 2005; Barenfeld et al. 2013). The spectra coincide in the overall shapes and in the depth of the oxide bands, suggesting that they may have similar temperatures and gravities. The most remarkable difference between our target and these comparison spectra in the optical is the Hα emission line, which is strong in 2MASS J0249−0557 c but it is not detected in either 2MASS 0045+1634 or G 196–3B (Mohanty & Basri 2003). We discuss this in more detail in section 5.4.

We have also computed spectral indices from Martín et al. (1999) to assess the spectral classification of this target. They are listed in Table 3. We excluded other commonly used indices related to the oxides because these features are strongly affected by gravity and are not adequate for spectral type determination
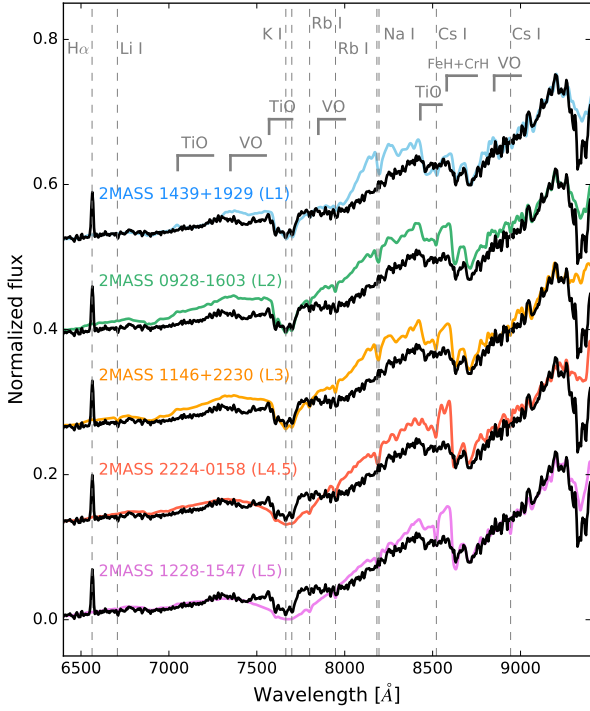
Fig. 4. GTC/OSIRIS optical spectrum of 2MASS J0249−0557 c (black) compared to old field optical L standards from Kirkpatrick et al. (1999) and Kirkpatrick et al. (2000) observed with Keck-I/LRIS (coloured). LRIS spectra were convolved with a Gaussian to match the OSIRIS spectrum resolution. Spectra were normalised at wavelength ∼9200 Å and shifted by a constant for clarity. Several spectral features are marked in grey.

Table 3. Spectral indices for spectral type determination.

Index	Value	SpT	Index Ref.[a]
Optical			
PC3	2.78	L1.5±0.5	M99
PC6	21.9	M8–L4	M99
Infrared			
H_2O [b]	1.35	L4±0.5	A07
H_2OD [b]	0.99	L0.25±0.75	ML03
H_2O-1 [b]	0.59	L3.25±1.00	S04
H_2O-2 [b]	0.82	L1.25±0.50	S04

Notes. [a] References: A07 – Allers et al. (2007), M99 – Martín et al. (1999), ML03 – McLean et al. (2003), S04 – Slesnick et al. (2004). [b] Results obtained using the Allers & Liu (2013) polynomial fits.

in young objects. Based on our comparison with young and field L dwarfs and the spectral indices, we finally adopted a classification in the optical of L2.5±0.5.

Fig. 5. GTC/OSIRIS optical spectrum of 2MASS J0249−0557 c (black) compared to other known young L objects (coloured) from Cruz et al. (2009, 2MASS 1022+5825, 2MASS 0501−0010 and 2MASS 0355+1133) and Zapatero Osorio et al. (2014, 2MASS 0045+1634 and G196–3B). The GTC/OSIRIS spectrum was convolved with Gaussians to match the young L1–L3 template spectra resolutions. For the L4–L5 comparisons, the template spectra were convolved to match the target spectral resolution. Spectra were normalised at wavelength ∼9200 Å and shifted by a constant for clarity. Some spectral features are marked in grey.

5.2. Infrared spectral classification

To determine the near-infrared spectral type, we compared our NTT/SofI spectrum with infrared spectra of known young and field objects. Figure 6 shows a comparison of our 2MASS J0249−0557 c near-infrared spectrum with several old field L dwarfs from Kirkpatrick et al. (1999) and Kirkpatrick et al. (2000). This figure shows that the spectral energy distribution of our target in the near-infrared bands resembles that of the L3 and L4.5 spectral types, except for the different shapes of the H band and the depth of some molecular bands such as VO and FeH, which are more intense in 2MASS J0249−0557 c. The triangular shape of the H band (e.g., Lucas et al. 2001; Allers & Liu 2013) is a remarkable feature that reveals the young nature of this object.

Figure 7 shows the near-infrared spectrum of 2MASS J0249−0557 c compared to very low gravity L spectral templates from Cruz et al. (2018). The spectrum fits the L2γ, L3γ, and L4γ templates in each of the individual near-infrared bands rather well. This is clearly visible in the slopes of the H_2O absorption bands at either side of the H band, and also at the red side of the J band. However, there are some discrepancies. For example, the VO band at 1.06 μm is stronger in 2MASS J0249−0557 c than
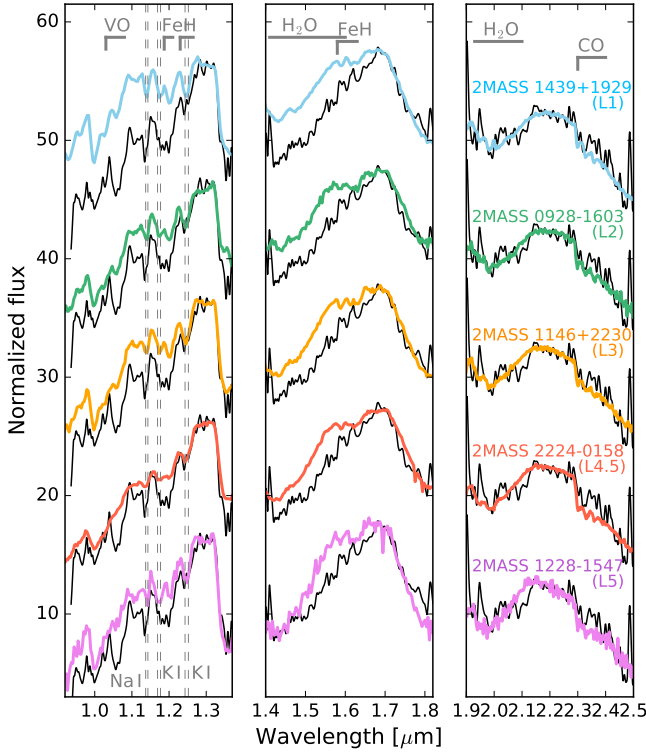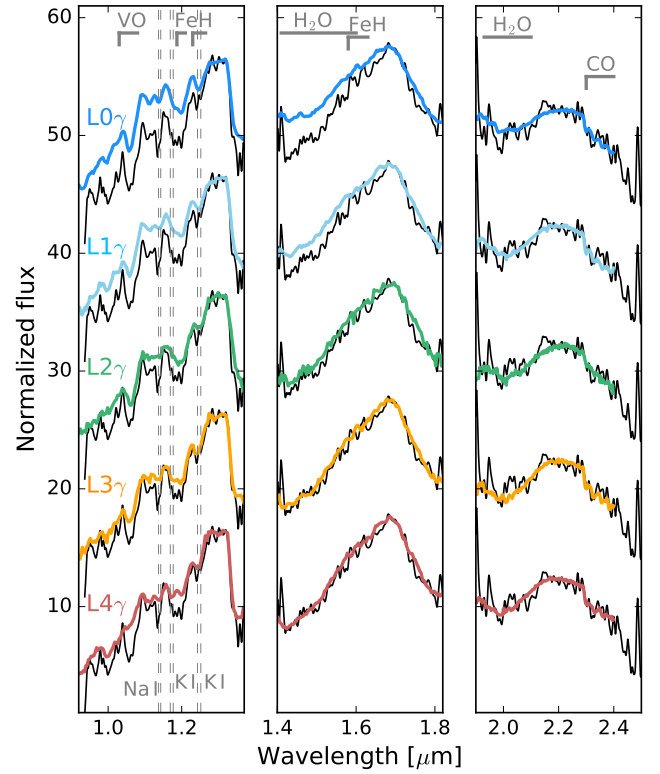
Fig. 6. NTT/SofI spectrum of 2MASS J0249−0557 c (black) compared to old field L standards from Kirkpatrick et al. (1999) and Kirkpatrick et al. (2000) observed with IRTF/SpeX (coloured) by Burgasser et al. (2004), Burgasser et al. (2010), and Cruz et al. (2018). The NTT/SofI spectrum was convolved with a Gaussian to match the resolution of SpeX spectra. *J, H,* and *K* bands are displayed and normalised separately. Some spectral features, such as the VO, FeH, H_2O, and CO bands or the NaI and KI doublets, are marked in grey.

in the templates. For an old object this would imply an earlier spectral type, but in this case, it may indicate a lower gravity, and hence a younger age for 2MASS J0249−0557 c compared to the templates. Although all the objects used to produce these template spectra show very low gravity features, and at least one of the three objects used to produce the L3γ template is probably a member of β Pic (see Cruz et al. 2018), they may have a wider range of ages and many of them may be older than this young moving group.

To confirm this spectral type classification, we also estimated the near-infrared spectral indices based on H_2O absorption bands from Allers et al. (2007), McLean et al. (2003) and Slesnick et al. (2004) and the best gravity-dependent indices defined by Lodieu et al. (2018) for the gravity type. These indices are shown in Table 3 and Table 4. Based on these comparisons and the spectral indices, we finally adopted a spectral type of L3±1 γ in the near-infrared for 2MASS J0249−0557 c, where the γ suffix is an indication of very low gravity features. This classification is compatible with the spectral type determination of L2±1 VL-G assigned by Dupuy et al. (2018), where VL-G also indicates a very low gravity. This is consistent with the signs of youth we have found in the optical and near-infrared spectra and with the expected age for a member of β Pic.

Fig. 7. Same as Fig. 6, but comparing the NTT/SofI spectrum of 2MASS J0249−0557 c (black) to near-infrared very low gravity L dwarf templates from Cruz et al. (2018) (coloured). The NTT/SofI spectrum was convolved with a Gaussian to match the spectral resolution of the templates.

Table 4. Gravity-dependent indices.

Index	Value	Gravity[a]	Index Ref.[b]
H-cont	0.99	γ	AL13
CH$_4$-H	1.16	β–γ	B06
VO$_z$	1.50	γ	AL13
H$_2$O-K	0.86	β–γ	B06

Notes. [a] Gravity indices as described in Kirkpatrick (2005) and Cruz et al. (2009). Assigned following the plots in Fig. A1 of Lodieu et al. (2018). [b] References: AL13 – Allers & Liu (2013), B06 – Burgasser et al. (2006)

5.3. Comparison between optical and near-infrared spectral classification

We adopted a spectral type of L3±1 in the near-infrared, which agrees well with previous determination by Dupuy et al. (2018), and L2.5±0.5 in the optical. This is the first classification of this object in this wavelength range. Although the uncertainty in the spectral type determination of young objects is larger than in older field L dwarfs because the low-gravity templates do not constitute a homogeneous sample of targets with the same age and hence evolutionary state, our classification in the optical and in the near-infrared is compatible.

Previous studies in very young open clusters and associations with ages younger than ∼ 10 Myr have shown that L dwarfs may have a slightly earlier spectral type in the optical than in the near-infrared (Zapatero Osorio et al. 2017; Lodieu et al. 2018). However, this does not seem to be the case for L dwarfs belonging to YMGs and associations at ages >10 Myr (Cruz et al. 2018). The β Pic group is close to the frontier between the two age groups and therefore is a favourable place to investigate this issue in more detail.

5.4. Hα emission in 2MASS J0249−0557 c

As pointed out in previous sections, the strong Hα emission line at 6563 Å is a remarkable feature of this object. To investigate the chromospheric activity and its variability, we measured the Hα pEW in the final combined GTC/OSIRIS spectrum by fitting a Gaussian profile to the line using the SPLOT task within the IRAF environment. We repeated this procedure several times, selecting a wide range of acceptable continuum levels. The average measured pEW is -90^{+20}_{-40}Å. The quoted error takes the spread of the measured pEWs with the different choices of the continuum level into account.

This object was also observed by the Extended Baryon Oscillation Spectroscopic Survey (eBOSS; Dawson et al. 2016) from the SDSS on 3 December 2015. This survey is carried out using the BOSS spectrographs (Smee et al. 2013) mounted on the SDSS 2.5m telescope (Gunn et al. 2006) at the Apache Point Observatory, New Mexico. The eBOSS optical spectral coverage is 3600–10400 Å, and the spectral resolution is 1300–2500 (Alam et al. 2015). The eBOSS spectra are publicly available in the SDSS Sky Server.[1] Due to the faintness of the object in the bluer range, the signal-to-noise ratio of the spectrum is rather poor in the Hα region, and the pseudo-continuum level is nearly zero. Nevertheless, the Hα emission line can be recognised. We measured a lower limit in the Hα emission of 20 Å from the eBOSS spectrum (pEW < −20Å).

The left panel of Figure 8 shows the comparison between the Hα lines of the eBOSS and the GTC/OSIRIS spectra of 2MASS J0249−0557 c. The time baseline between the observations is three years. This figure shows that the emission of Hα appears at both epochs. Although it is possible that we have observed the object during two isolated flare episodes by chance, it is therefore more likely that the Hα emission in 2MASS J0249−0557 c is persistent on timescales of years and is not related to episodic events.

We have also analysed the variations in the Hα emission within the individual exposures of the GTC/OSIRIS observations. Four exposures of 1600s (∼27 min) were taken. We extracted the individual spectra and measured the Hα pEW in each one of them separately. Table 5 shows the Hα measurements of the individual exposures and of the combined spectrum. The right panel of Figure 8 shows the comparison between the four individual exposures. We find consistent values of the Hα pEW in them, with some variations that do not seem to be significant within the errors. Because the pseudo-continuum flux of the target in the wavelength region around Hα is low, the measured errors of the pEW in the individual spectra are relatively large.
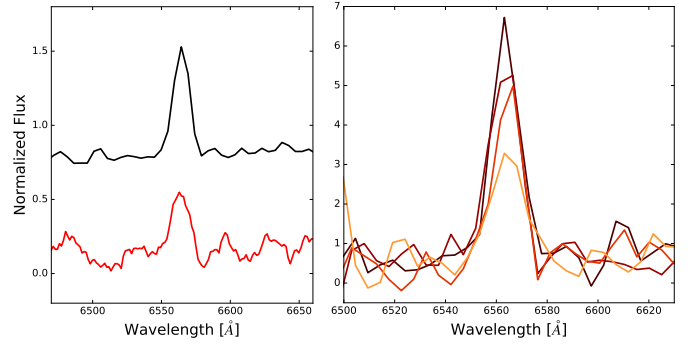
Fig. 8. Variation in the Hα emission line. The left panel shows the Hα line in our GTC/OSIRIS spectrum (black) compared with the eBOSS spectrum (red). The eBOSS spectrum has been smoothed for a better visualisation. The right panel shows the Hα line extracted from the four GTC/OSIRIS individual exposures separately.

Table 5. Hα measurements for 2MASS J0249−0557 c.

	MJD	Hα pEW (Å)
eBOSS	57359	< -20 [a]
OSIRIS Indiv. 1	58510.841	-110^{+40}_{-100}
OSIRIS Indiv. 2	58510.859	-110^{+40}_{-80}
OSIRIS Indiv. 3	58510.878	-130^{+70}_{-60} [b]
OSIRIS Indiv. 4	58510.897	-80^{+40}_{-70}
OSIRIS Comb.	58510.87	-90^{+20}_{-40}

Notes. [a] The pseudo-continuum emission in the Hα region is too close to zero in this spectrum. [b] Very low continuum level in the Hα region.

5.5. Hα emission in ultra-cool dwarfs

The Hα line found in emission in ultra-cool dwarfs is usually associated with chromospheric activity and/or accretion (Hawley et al. 1996; Gizis et al. 2000; White & Basri 2003; Mohanty & Basri 2003; Muzerolle et al. 2003; Jayawardhana et al. 2003; Mohanty et al. 2005; Caballero et al. 2006). It is a common feature in late-M and early-L objects and occurs most frequently at ~M7 spectral type. It decreases dramatically for mid-L and later spectral types (Gizis et al. 2000; Schmidt et al. 2015; Pineda et al. 2016). In addition, although some old L-type objects may present Hα emission lines due to flares and close binarity, a strong and stable Hα emission is commonly associated with youth (Liebert et al. 2003). However, many known young objects lack Hα emission (e.g. Martín et al. 2010; Lodieu et al. 2018; Chinchilla et al. 2020). Stable and strong Hα emission therefore is a sufficient but not necessary indicator of youth.

We can find many examples of young late-M brown dwarfs with strong Hα in emission in open clusters and associations of different ages (e.g. Luhman et al. 1997; Béjar et al. 1999; Luhman 1999; Ardila et al. 2000; Comerón et al. 2000; Martín et al. 2001; Briceño et al. 2002; Zapatero Osorio et al. 2002b; Barrado y Navascués & Martín 2003; White & Basri 2003; Mohanty et al. 2005; Lodieu et al. 2006; Slesnick et al. 2006; Barrado y Navascués et al. 2007; Lodieu et al. 2011). However, there are very few young L-dwarfs with a pronounced Hα emis-

sion. An outstanding case is 2MASS J11151597+1937266, an L2γ in the planetary mass regime with a strong Hα emission (pEW=560±82 Å, Theissen et al. 2017, 2018). In Sigma Orionis (1–8 Myr; Zapatero Osorio et al. 2002b), S Ori 71, a young L0 brown dwarf was reported to have an Hα pEW of around −700 Å (Barrado y Navascués et al. 2002). A similar case in this open cluster is S Ori 55, a substellar M9 object at the deuterium-burning mass limit with a variable Hα with pEW of 180–410 Å (Zapatero Osorio et al. 2002a). In these two cases the presence of strong Hα emission is attributed to the presence of an accretion disk, mass transfer in a binary system, or flare activity. Finally, although many late-M dwarfs in the Upper Scorpius (∼5–10 Myr) association have strong Hα emission, only a few of the early L-type objects of this region also present noticeable Hα emission, such as VISTA J1607−2146, VISTA J1611−2215, and VISTA 1615−2229 (Lodieu et al. 2018).

In addition, some candidate young exoplanets still in their formation stage have been found to present strong Hα emission, probably caused by accretion. This is the case of PDS 70 b and c (Wagner et al. 2018; Haffert et al. 2019), and LkCa15 (Kraus & Ireland 2012; Sallum et al. 2015), although recent studies showed that the Hα emission in this last object may come from an inner disk structure and not from a planet (Thalmann et al. 2016; Mendigutía et al. 2018; Currie et al. 2019). Some techniques have been proposed for using this Hα emission as a resource to detect new young exoplanets, such as spectro-astrometry (Mendigutía et al. 2018), or adaptive optics imaging in the Hα band (e.g. Close et al. 2014; Huélamo et al. 2018; Cugno et al. 2019; Zurlo et al. 2020).

2MASS J0249−0557 c is very similar in age, mass, and temperature to the planet β Pic b (Lagrange et al. 2010). This object may therefore show a similarly strong Hα emission. On the other hand, another similar wide companion in the β Pic moving group is 2MASS J21265040−8140293. This object has a spectral type of L3 and orbits the β Pic candidate member TYC 9486-927-1 at a separation of > 4500 AU (Deacon et al. 2016).[2] However, 2MASS J21265040−8140293 does not show any remarkable Hα emission (pEW > −15Å) in its optical spectrum (Cruz et al. 2007)[3]. The planet β Pic b has only been spectroscopically observed in the near-infrared (Chilcote et al. 2017), and no optical spectrum has been obtained so far. The possibility of an Hα emission in this planetary mass object therefore has not been tested yet.

In conclusion, strong Hα emission such as is observed in 2MASS J0249−0557 c is uncommon among old field L dwarfs, but several cases of young L-type objects exhibiting Hα emission at similar strength are known. However, in most of these examples, the objects are younger than 10 Myr, and this may be related to the presence of accretion disks. At the age of the β Pic (∼20–25 Myr), the gas in the disks is expected to have dissipated (Haisch et al. 2001). Nevertheless, this may not be the case for lower mass substellar objects, which may have longer disk-decay timescales (Riaz & Gizis 2008). Some cases of β Pic brown dwarf members show signs of the presence of a disk and ongoing accretion (e.g. 2M0335+23, 2M1935−28; Shkolnik et al. 2009, 2012; Liu et al. 2016), therefore this possibility cannot be ruled out. The lack of IR excess in the *WISE* w1 and w2 photometry of the object (see Table 1) indicates the absence of

a warm disk around it. However, although the origin of the Hα emission may be chromospheric, we cannot rule out a colder disk of material or the possibility of gas accretion in the object. As an example, some of the planetary mass objects with signs of accretion in Sigma Orionis, such as S Ori 55, only show infrared excesses at wavelengths longer than 5 microns (Zapatero Osorio et al. 2007a).

5.6. Binding energy and tidal disruption

Widely separated systems, especially those with low binding energies, are prone to disruption by external perturbations, such as close encounters with other stars (Kroupa 1995; Close et al. 2007). This is the case of the 2MASS J0249−0557 c component.

We calculated the binding energy of the system, as described in Chinchilla et al. (2020). Masses and separations were obtained from Dupuy et al. (2018). We infer an (absolute) upper limit for the binding energy of 2MASS J0249−0557 c of $U = (−8.8 ± 4.4)10^{32}$ J. This result considers an orbital semi-major axis equal to the current observed separation. However, the actual semi-major axis may be larger due to projection effects. When we consider an average semi-major axis of $\langle a_{rel}\rangle = 1.26\,d\,\langle\alpha\rangle$ (Fischer & Marcy 1992), where d is the heliocentric distance and $\langle\alpha\rangle$ is the average observed angular separation of the components, the binding energy would become $U ∼ (−7.0 ± 3.4)10^{32}$ J. This binding energy is surprisingly low and makes this system one of the most fragile wide systems discovered up to date. Figure 9 shows the binding energy of 2MASS J0249−0557 AB(c) in comparison with other very wide (>1000 AU) binaries, exoplanets, and the planets of our Solar System. This figure shows that 2MASS J0249−0557 AB(c) is one of the substellar companions with the lowest binding energy known to date.

In order to estimate the time that this system is expected to survive in its actual environment, we calculated the expected disruption time using the relations from Binney & Tremaine (1987) and Weinberg et al. (1987), also as described in Chinchilla et al. (2020). We considered a similar mean velocity dispersion as the solar neighbourhood, calculated using the data in Zapatero Osorio et al. (2007b); we obtain a value of 52.8 km s^{-1}. To obtain the density of stars around the system, we used *Gaia* DR2 to select all the objects in a sphere of 8 pc radius around the system. We found 138 objects in this volume, which corresponds to a density of 0.064 obj pc^{-3}. Using these values, we obtain an estimated disruption time of 4–14 Gyr. We must consider that this system may have formed in a denser environment, similar to young forming regions and associations. Considering a higher density of objects (∼10 obj pc^{-3}), we obtain a disruption time of 30–60 Myr for this system. These two results combined indicate that the system may have been formed in the outskirts of a young open cluster or stellar association, being physically bound since then, and that it will probably survive to ages similar to that of our Solar System. It is interesting to note that 2MASS J0249−0557 c, with an estimated mass of ∼12 M$_{Jup}$, will have a temperature of ∼ 500 K at the age of the Sun, within the Y dwarf spectral type range, which makes the detection of similar systems at these old ages very difficult with current means. The James Webb Space Telescope (JWST), with its near. and mid-infrared capabilities, may be able to identify these types of objects.

6. Summary and final remarks

We presented the independent identification of 2MASS J0249−0557 c: a wide (2640±20 AU) substellar com-

---

[2] As pointed out in Deacon et al. (2016), this system is also compatible with the Tucana-Horologium association. However, it most likely belongs to the β Pic association.

[3] Spectrum available at the BDNYC database in http://database.bdnyc.org/browse
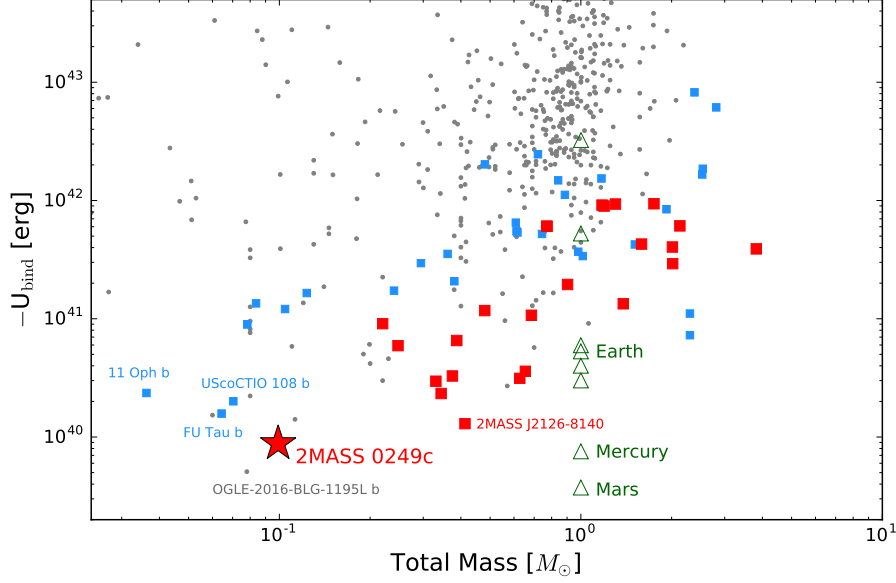
Fig. 9. Binding energy compared to the total mass of the system for known substellar companions, including planets and brown dwarfs. The binding energy of 2MASS J0249−0557 c is marked with a red star. Other substellar companions with separations >1000 AU are marked as red squares (masses and separations from Chinchilla et al. (2020) and references therein). Objects with orbital separations <100 AU are marked as grey dots, and objects with separations between 100–1000 AU are marked as small blue squares (masses and separations from The Extrasolar Planets Encyclopaedia[4]; Schneider et al. (2011)). The binding energies of the Solar System planets are also included, marked as green triangles.

panion of the binary brown dwarfs 2MASS J0249−0557 AB, recently discovered by Dupuy et al. (2018). We found this candidate companion in our proper motion search around YMG members by combining the astrometry and photometry of the VHS and 2MASS catalogues, and using photometry from other catalogues such as DENIS and/or AllWise, and astrometry from *Gaia* DR2, when available.

We acquired optical and near-infrared spectroscopy of 2MASS J0249−0557 c to characterise its spectral energy distribution and atmospheric properties. We assigned a spectral type of L2.5±0.5 in the optical and L3±1 in the near-infrared. This spectral classification is consistent with that of Dupuy et al. (2018).

We found spectral features characteristic of youth, such as strong Hα emission in the optical, a peaked shape in the *H* band, weak alkaline lines, and strong VO, TiO, and FeH bands both in the optical and near-infrared. We observe a tentative Li I detection with a pEW of $\lesssim 5$ Å. These features are consistent with the very low gravity classification by Dupuy et al. (2018) and with the expected membership in β Pic.

2MASS J0249−0557 c shows a strong Hα emission line, with a pEW of -90^{+20}_{-40}, which is likely stable on timescales of hours and years. This emission is not very common among old field L dwarfs, but it may be present in some of the young early-L dwarfs, especially those located in regions of ages younger than 10 Myr. This reinforces the young age of 2MASS J0249−0557 c.

With an (absolute) upper limit of $U = (−8.8 \pm 4.4)10^{32}$J, 2MASS J0249−0557 AB(c) is one of the widest low-mass systems with the lowest binding energy known to date. It may have been formed in the outskirts of a young star formation region and it is expected to survive at ages similar to our Solar System.

The solar vicinity may be populated by similar systems, but they may have remained unnoticed with current facilities.

References

Alam, S., Albareti, F. D., Allende Prieto, C., et al. 2015, ApJS, 219, 12
Aller, K. M., Kraus, A. L., Liu, M. C., et al. 2013, ApJ, 773, 63
Allers, K. N., Jaffe, D. T., Luhman, K. L., et al. 2007, ApJ, 657, 511

---

[4] http://exoplanet.eu

Allers, K. N. & Liu, M. C. 2013, ApJ, 772, 79
Ardila, D., Martín, E., & Basri, G. 2000, AJ, 120, 479
Barenfeld, S. A., Bubar, E. J., Mamajek, E. E., & Young, P. A. 2013, ApJ, 766, 6
Barrado y Navascués, D. & Martín, E. L. 2003, AJ, 126, 2997
Barrado y Navascués, D., Stauffer, J. R., Morales-Calderón, M., et al. 2007, ApJ, 664, 481
Barrado y Navascués, D., Stauffer, J. R., Song, I., & Caillault, J. P. 1999, ApJ, 520, L123
Barrado y Navascués, D., Zapatero Osorio, M. R., Martín, E. L., et al. 2002, A&A, 393, L85
Béjar, V. J. S., Zapatero Osorio, M. R., & Rebolo, R. 1999, ApJ, 521, 671
Bell, C. P. M., Mamajek, E. E., & Naylor, T. 2015, MNRAS, 454, 593
Best, W. M. J., Liu, M. C., Magnier, E. A., et al. 2015, ApJ, 814, 118
Binks, A. S. & Jeffries, R. D. 2014, MNRAS, 438, L11
Binney, J. & Tremaine, S. 1987, Galactic dynamics
Bowler, B. P., Liu, M. C., Kraus, A. L., & Mann, A. W. 2014, ApJ, 784, 65
Briceño, C., Luhman, K. L., Hartmann, L., Stauffer, J. R., & Kirkpatrick, J. D. 2002, ApJ, 580, 317
Burgasser, A. J., Cruz, K. L., Cushing, M., et al. 2010, ApJ, 710, 1142
Burgasser, A. J., Geballe, T. R., Leggett, S. K., Kirkpatrick, J. D., & Golimowski, D. A. 2006, ApJ, 637, 1067
Burgasser, A. J., McElwain, M. W., Kirkpatrick, J. D., et al. 2004, AJ, 127, 2856
Caballero, J. A., Martín, E. L., Zapatero Osorio, M. R., et al. 2006, A&A, 445, 143
Cepa, J., Aguiar, M., Escalera, V. G., et al. 2000, in Proc. SPIE, Vol. 4008, Optical and IR Telescope Instrumentation and Detectors, ed. M. Iye & A. F. Moorwood, 623–631
Chambers, K. C., Magnier, E. A., Metcalfe, N., et al. 2016, arXiv e-prints, arXiv:1612.05560
Chilcote, J., Pueyo, L., De Rosa, R. J., et al. 2017, AJ, 153, 182
Chinchilla, P., Béjar, V. J. S., Lodieu, N., et al. 2020, A&A, 633, A152
Close, L. M., Follette, K. B., Males, J. R., et al. 2014, ApJ, 781, L30
Close, L. M., Zuckerman, B., Song, I., et al. 2007, ApJ, 660, 1492
Comerón, F., Neuhäuser, R., & Kaas, A. A. 2000, A&A, 359, 269
Cruz, K. L., Kirkpatrick, J. D., & Burgasser, A. J. 2009, AJ, 137, 3345
Cruz, K. L., Núñez, A., Burgasser, A. J., et al. 2018, AJ, 155, 34
Cruz, K. L., Reid, I. N., Kirkpatrick, J. D., et al. 2007, AJ, 133, 439
Cugno, G., Quanz, S. P., Hunziker, S., et al. 2019, A&A, 622, A156
Currie, T., Marois, C., Cieza, L., et al. 2019, ApJ, 877, L3
Dawson, K. S., Kneib, J.-P., Percival, W. J., et al. 2016, AJ, 151, 44
Deacon, N. R., Liu, M. C., Magnier, E. A., et al. 2014, ApJ, 792, 119
Deacon, N. R., Schlieder, J. E., & Murphy, S. J. 2016, MNRAS, 457, 3191
Dupuy, T. J. & Liu, M. C. 2012, ApJS, 201, 19
Dupuy, T. J., Liu, M. C., Allers, K. N., et al. 2018, AJ, 156, 57
Elliott, P., Bayo, A., Melo, C. H. F., et al. 2016, A&A, 590, A13
Epchtein, N., de Batz, B., Capoani, L., et al. 1997, The Messenger, 87, 27
Fischer, D. A. & Marcy, G. W. 1992, ApJ, 396, 178
Gagné, J. & Faherty, J. K. 2018, ApJ, 862, 138
Gagné, J., Faherty, J. K., Cruz, K. L., et al. 2015a, ApJS, 219, 33
Gagné, J., Lafrenière, D., Doyon, R., Malo, L., & Artigau, É. 2014, ApJ, 783, 121
Gagné, J., Lafrenière, D., Doyon, R., Malo, L., & Artigau, É. 2015b, ApJ, 798, 73
Gaia Collaboration, Brown, A. G. A., Vallenari, A., et al. 2018, A&A, 616, A1
Gaia Collaboration, Prusti, T., de Bruijne, J. H. J., et al. 2016, A&A, 595, A1
Gauza, B., Béjar, V. J. S., Pérez-Garrido, A., et al. 2015, ApJ, 804, 96
Gebbinck, M. K. & Sforna, D. 2007, Gasgano User's Manual, 66
Gizis, J. E., Monet, D. G., Reid, I. N., et al. 2000, AJ, 120, 1085
Gunn, J. E., Siegmund, W. A., Mannery, E. J., et al. 2006, AJ, 131, 2332
Haffert, S. Y., Bohn, A. J., de Boer, J., et al. 2019, Nature Astronomy, 3, 749
Haisch, Karl E., J., Lada, E. A., & Lada, C. J. 2001, ApJ, 553, L153
Hawley, S. L., Gizis, J. E., & Reid, I. N. 1996, AJ, 112, 2799
Huélamo, N., Chauvin, G., Schmid, H. M., et al. 2018, A&A, 613, L5
Jayawardhana, R., Mohanty, S., & Basri, G. 2003, ApJ, 592, 282
Kirkpatrick, J. D. 2005, ARA&A, 43, 195
Kirkpatrick, J. D., Reid, I. N., Liebert, J., et al. 1999, ApJ, 519, 802
Kirkpatrick, J. D., Reid, I. N., Liebert, J., et al. 2000, AJ, 120, 447
Kraus, A. L. & Ireland, M. J. 2012, ApJ, 745, 5
Kroupa, P. 1995, MNRAS, 277, 1522
Lagrange, A. M., Bonnefoy, M., Chauvin, G., et al. 2010, Science, 329, 57
Liebert, J., Kirkpatrick, J. D., Cruz, K. L., et al. 2003, AJ, 125, 343
Liu, M. C., Dupuy, T. J., & Allers, K. N. 2016, ApJ, 833, 96
Lodieu, N., Dobbie, P. D., & Hambly, N. C. 2011, A&A, 527, A24
Lodieu, N., Hambly, N. C., & Jameson, R. F. 2006, MNRAS, 373, 95
Lodieu, N., Pérez-Garrido, A., Béjar, V. J. S., et al. 2014, A&A, 569, A120
Lodieu, N., Zapatero Osorio, M. R., Béjar, V. J. S., & Peña Ramírez, K. 2018, MNRAS, 473, 2020

Lucas, P. W., Roche, P. F., Allard, F., & Hauschildt, P. H. 2001, MNRAS, 326, 695
Luhman, K. L. 1999, ApJ, 525, 466
Luhman, K. L., Liebert, J., & Rieke, G. H. 1997, ApJ, 489, L165
Luhman, K. L., Stauffer, J. R., & Mamajek, E. E. 2005, ApJ, 628, L69
Malo, L., Doyon, R., Feiden, G. A., et al. 2014, ApJ, 792, 37
Malo, L., Doyon, R., Lafrenière, D., et al. 2013, ApJ, 762, 88
Mamajek, E. E. & Bell, C. P. M. 2014, MNRAS, 445, 2169
Martín, E. L., Delfosse, X., Basri, G., et al. 1999, AJ, 118, 2466
Martín, E. L., Dougados, C., Magnier, E., et al. 2001, ApJ, 561, L195
Martín, E. L., Phan-Bao, N., Bessell, M., et al. 2010, A&A, 517, A53
McLean, I. S., McGovern, M. R., Burgasser, A. J., et al. 2003, ApJ, 596, 561
McMahon, R. G., Banerji, M., Gonzalez, E., et al. 2013, The Messenger, 154, 35
Mendigutía, I., Oudmaijer, R. D., Schneider, P. C., et al. 2018, A&A, 618, L9
Mentuch, E., Brandeker, A., van Kerkwijk, M. H., Jayawardhana, R., & Hauschildt, P. H. 2008, ApJ, 689, 1127
Messina, S., Lanzafame, A. C., Malo, L., et al. 2017, A&A, 607, A3
Miret-Roig, N., Antoja, T., Romero-Gómez, M., & Figueras, F. 2018, A&A, 615, A51
Mohanty, S. & Basri, G. 2003, ApJ, 583, 451
Mohanty, S., Jayawardhana, R., & Basri, G. 2005, ApJ, 626, 498
Moorwood, A., Cuby, J.-G., & Lidman, C. 1998, The Messenger, 91, 9
Muzerolle, J., Hillenbrand, L., Calvet, N., Briceño, C., & Hartmann, L. 2003, ApJ, 592, 266
Pecaut, M. J. & Mamajek, E. E. 2013, ApJS, 208, 9
Pineda, J. S., Hallinan, G., Kirkpatrick, J. D., et al. 2016, ApJ, 826, 73
Rebolo, R., Zapatero Osorio, M. R., Madruga, S., et al. 1998, Science, 282, 1309
Riaz, B. & Gizis, J. E. 2008, ApJ, 681, 1584
Sallum, S., Follette, K. B., Eisner, J. A., et al. 2015, Nature, 527, 342
Schlieder, J. E., Lépine, S., & Simon, M. 2010, AJ, 140, 119
Schlieder, J. E., Lépine, S., & Simon, M. 2012, AJ, 144, 109
Schmidt, S. J., Hawley, S. L., West, A. A., et al. 2015, AJ, 149, 158
Schneider, A. C., Windsor, J., Cushing, M. C., Kirkpatrick, J. D., & Shkolnik, E. L. 2017, AJ, 153, 196
Schneider, J., Dedieu, C., Le Sidaner, P., Savalle, R., & Zolotukhin, I. 2011, A&A, 532, A79
Shkolnik, E., Liu, M. C., & Reid, I. N. 2009, ApJ, 699, 649
Shkolnik, E. L., Allers, K. N., Kraus, A. L., Liu, M. C., & Flagg, L. 2017, AJ, 154, 69
Shkolnik, E. L., Anglada-Escudé, G., Liu, M. C., et al. 2012, ApJ, 758, 56
Skrutskie, M. F., Cutri, R. M., Stiening, R., et al. 2006, AJ, 131, 1163
Slesnick, C. L., Carpenter, J. M., & Hillenbrand, L. A. 2006, AJ, 131, 3016
Slesnick, C. L., Hillenbrand, L. A., & Carpenter, J. M. 2004, ApJ, 610, 1045
Smee, S. A., Gunn, J. E., Uomoto, A., et al. 2013, AJ, 146, 32
Thalmann, C., Janson, M., Garufi, A., et al. 2016, ApJ, 828, L17
Theissen, C. A., Burgasser, A. J., Bardalez Gagliuffi, D. C., et al. 2018, ApJ, 853, 75
Theissen, C. A., West, A. A., Shippee, G., Burgasser, A. J., & Schmidt, S. J. 2017, AJ, 153, 92
Tody, D. 1986, in Proc. SPIE, Vol. 627, Instrumentation in astronomy VI, ed. D. L. Crawford, 733
Tody, D. 1993, in Astronomical Society of the Pacific Conference Series, Vol. 52, Astronomical Data Analysis Software and Systems II, ed. R. J. Hanisch, R. J. V. Brissenden, & J. Barnes, 173
Torres, C. A. O., Quast, G. R., Melo, C. H. F., & Sterzik, M. F. 2008, Young Nearby Loose Associations, ed. B. Reipurth, Vol. 5, 757
Wagner, K., Follete, K. B., Close, L. M., et al. 2018, ApJ, 863, L8
Weinberg, M. D., Shapiro, S. L., & Wasserman, I. 1987, ApJ, 312, 367
White, R. J. & Basri, G. 2003, ApJ, 582, 1109
Wright, E. L., Eisenhardt, P. R. M., Mainzer, A. K., et al. 2010, AJ, 140, 1868
York, D. G., Adelman, J., Anderson, Jr., J. E., et al. 2000, AJ, 120, 1579
Zapatero Osorio, M. R., Béjar, V. J. S., Martín, E. L., Barrado y Navascués, D., & Rebolo, R. 2002a, ApJ, 569, L99
Zapatero Osorio, M. R., Béjar, V. J. S., Miles-Páez, P. A., et al. 2014, A&A, 568, A6
Zapatero Osorio, M. R., Béjar, V. J. S., Pavlenko, Y., et al. 2002b, A&A, 384, 937
Zapatero Osorio, M. R., Béjar, V. J. S., & Peña Ramírez, K. 2017, ApJ, 842, 65
Zapatero Osorio, M. R., Caballero, J. A., Béjar, V. J. S., et al. 2007a, A&A, 472, L9
Zapatero Osorio, M. R., Martín, E. L., Béjar, V. J. S., et al. 2007b, ApJ, 666, 1205
Zapatero Osorio, M. R., Rebolo, R., Bihain, G., et al. 2010, ApJ, 715, 1408
Zuckerman, B. 2019, ApJ, 870, 27
Zuckerman, B., Song, I., & Bessell, M. S. 2004, ApJ, 613, L65
Zuckerman, B., Song, I., Bessell, M. S., & Webb, R. A. 2001, ApJ, 562, L87
Zurlo, A., Cugno, G., Montesinos, M., et al. 2020, A&A, 633, A119